# Treatment Effect of Balloon Pulmonary Angioplasty in CTEPH, Quantified by Automatic Comparative Imaging in CTPA

Zhiwei Zhai, MS[1], Hideki Ota, MD, PhD[2], Marius Staring, PhD[1], Jan Stolk, MD, PhD[3], Koichiro Sugimura, MD, PhD[4], Kei Takase, MD, PhD[2], Berend C. Stoel, PhD[1]

[1] Division of Image Processing, Department of Radiology,
Leiden University Medical Center, the Netherlands
[2] Department of Diagnostic Radiology
Tohoku University Hospital, Japan
[3] Department of Pulmonology
Leiden University Medical Center, the Netherlands
[4] Department of Cardiology
Tohoku University Hospital, Japan

## ABSTRACT

**Objectives**: Balloon pulmonary angioplasty (BPA) in patients with inoperable chronic thromboembolic pulmonary hypertension (CTEPH) can have variable outcomes. To gain more insight into this variation, we designed a method for visualizing and quantifying changes in pulmonary perfusion by automatically comparing CT pulmonary angiography (CTPA) before and after BPA treatment. We validated these quantifications of perfusion changes against hemodynamic changes measured with right-heart catheterization (RHC).

**Materials and Methods**: We studied 14 consecutive CTEPH patients (12 females; age:70.5 ± 24), who underwent CTPA and RHC, before and after BPA. Post-treatment images were registered to pre-treatment CT scans (using the Elastix toolbox) to obtain corresponding locations. Pulmonary vascular trees and their centerlines were detected using a graph-cuts method and a distance transform method, respectively. Areas distal from vessels were defined as pulmonary parenchyma. Subsequently, the density changes within the vascular centerlines and parenchymal areas were calculated and corrected for inspiration level differences. For visualization, the densitometric changes were displayed in color-coded overlays. For quantification, the median and inter-quartile range (IQR) of the density changes in the vascular and parenchymal areas (ΔVD and ΔPD) were calculated. The recorded changes in hemodynamic parameters, including changes in systolic, diastolic, mean pulmonary artery pressure (ΔsPAP, ΔdPAP and ΔmPAP, respectively) and vascular resistance (ΔPVR),

were used as reference assessments of the treatment effect. Spearman's correlation coefficients were employed to investigate the correlations between changes in perfusion and hemodynamic changes.

**Results**: Comparative imaging maps showed distinct patterns in perfusion changes among patients. Within pulmonary vessels, the IQR of ΔVD correlated significantly with ΔsPAP (R=-0.58, p=0.03), ΔdPAP (R=-0.71, p=0.005), ΔmPAP (R=-0.71, p=0.005) and ΔPVR (R=-0.77, p=0.001). In the parenchyma, the median of ΔPD had significant correlations with ΔdPAP (R=-0.58, p=0.030) and ΔmPAP (R=-0.59, p=0.025).

**Conclusions**: Comparative imaging analysis in CTEPH patients offers insight into differences in BPA treatment effect. Quantification of perfusion changes provides non-invasive measures that reflect hemodynamic changes.

**Keywords:** chronic thromboembolic pulmonary hypertension, balloon pulmonary angioplasty, computed tomography, imaging quantifications

## Introduction

Chronic thromboembolic pulmonary hypertension (CTEPH) is caused by persistent obstruction of pulmonary arteries following pulmonary embolism (1). The mechanical obstruction of pulmonary arterials is produced by fibrotic transformation of pulmonary thrombus (2), which could lead to pulmonary hypertension and increasing pulmonary vascular resistance (PVR). Without treatment, CTEPH patients have poor prognoses: 2-years survival rate is less than 50% in patients with mean pulmonary artery pressure (PAP) > 30 mmHg (3, 4). The prognosis can be improved by pulmonary endarterectomy (PEA) (5) or balloon pulmonary angioplasty (BPA) (6), combined with optimal medications. PEA is the curative treatment for CTEPH, with nearly normalized hemodynamics in the majority of patients (7). However, for patients with inoperable CTEPH, BPA can be an alternative treatment to improve the clinical status and hemodynamics with a low mortality (8).

Evaluation of disease severity and assessment of treatment effects play an important role in the therapy of CTEPH. In evaluating the severity of CTEPH and assessing treatment effects, invasive right-heart

catheterization (RHC) serves as gold standard (9). The 6-min walk distance (6MWD) (10) and the brain natriuretic peptide (BNP) level (11) are the most frequently used non-invasive measurements to quantify treatment effect. Non-invasive imaging techniques play a key role in both diagnosis of CTEPH and assessment of the treatment effect (2). Radionuclide ventilation/perfusion (VQ) scans are recommended as an initial step in the diagnosis of CTEPH (9), but it is difficult to quantify treatment effects with VQ scans. CT pulmonary angiography (CTPA) is used in the evaluation of severity of CTEPH (12). Compared with conventional pulmonary angiography, CTPA has benefits for providing additional details in high-resolution 3D images (13). Recently, dual-energy CT has shown its capability in visualizing pulmonary vascular disease and assessing severity of CTEPH (14, 15).

BPA treatment can improve the hemodynamics of pulmonary vascular systems (8) and may contribute to the improvements of pulmonary vascular and parenchymal perfusion. We hypothesized that the perfusion changes achieved by BPA might reflect densitometric changes in CTPA. Thus, an objective and automatic method was designed to quantify the density changes in pulmonary vascular and parenchymal areas by comparatively analyzing CTPA before and after BPA. Moreover, we validated these image quantifications of perfusion changes against hemodynamic changes measured via RHC.

# Materials and Methods

## Patients

We studied a cohort of 14 consecutive patients (age, 70.5 ± 24, including 12 females) who were diagnosed with inoperable CTEPH and were treated with BPA between May 2013 and April 2016, referred to the Tohoku University Hospital. All studied patients underwent both CTPA and RHC examinations, before and after BPA treatment. All patients underwent several sessions of BPA procedures besides standard medication such as anticoagulants and vasodilators. As a vasodilator for symptoms prior to BPA, Riociguat, Tadarafil, Ambrisentan and Beraprost were used in 7, 5, 2 and 2 patients, respectively. During one procedure, the target lesion was limited to one or two segments in one lobe to minimize complications of BPA. We repeated BPA sessions at a

4–8 weeks interval (6). Seven patients underwent the initial CTPA scan before the first BPA session; the other seven subjects had undergone a part of BPA sessions before the initial CTPA scan. The number of BPA sessions between the two CTPA exams ranged between 1 and 4 (median: 3). The intervals between CTPA and RHC were 0 to 37 days (median: 2 days). This prospective study was approved by the local ethics committee, and written informed consent was obtained from all patients.

All patients were scanned with a second generation dual-source CT scanner (SOMATOM Definition Flash; Siemens Healthcare GmbH, Forchheim, Germany) with inspirational breath-hold and contrast enhancement. Contrast enhancement containing 350 mg/mL iodine was injected at a speed of 0.075 mL/s/kg × body-weight (in kg) over a period of 6 s, and subsequently a 40 mL saline flush was delivered at the same injection speed via a 20-gauge intravenous catheter, placed in the right antecubital vein using a double-headed power injector. A test injection technique was used to determine the scan delay: 12 mL iodine-containing contrast medium followed by 20 mL saline. For each patient, a region of interest (ROI) was placed within main pulmonary artery and the time-density curve within the ROI was recorded. The dual-source CT scan commenced 1 s after the test injection-mediated enhancement peaked (15). The X-ray tube settings (with automatic tube current modulation) were for tube A: voltage 80 kVp with a quality reference mAs of 141; and for tube B with a tin (Sn) filter: 140 kVp with a quality reference mAs of 60. Gantry rotation speed was 0.28 s per rotation, collimation 64 × 0.6 mm, pitch 1.00. Data was reconstructed with a slice thickness of 1 mm using a standard soft-tissue iterative reconstruction kernel (I30f, Sinogram Affirmed Iterative Reconstruction, [SAFIRE], strength 3). The 80 kVp and 140 kVp voltage images were fused into mixed images with a single energy of 120 kVp and with a mixing ratio of 0.6 : 0.4, using the dual-energy application software on a commercially available workstation (syngo CT Workplace, VA44A; Siemens Healthcare GmbH) (15). Only the mixed CTPA images were investigated in this study.

The hemodynamic parameters were examined at the main pulmonary artery via RHC in all patients both before and after BPA treatment. These included PAP (systolic, diastolic and mean), systolic right ventricular pressure (RVP), right atrial pressure (RAP), cardiac output (CO), cardiac index (CI) and pulmonary capillary wedge pressure (PCWP). The PVR was calculated using the following formula: PVR = (mean PAP − PCWP)/CO × 80 (dyne·s/cm$^5$) (16). The RHC examinations were used as gold standard to evaluate the severity

of CTEPH (9), the changes in PAP (ΔsPAP, ΔdPAP and ΔmPAP) and in PVR (ΔPVR) after BPA treatment were calculated as the reference assessments for the treatment effects. 6MWD data were recorded for 13 out of 14 patients. BNP and mean transit time (MTT) were collected for all patients. The diameter of the pulmonary artery (PA) trunk was measured on axial images. Short axis measurements of the left and right ventricle (LV and RV, resp.) were performed in 4-chamber images, and the ratio between RV and LV short axes (RV/LV) was calculated. The interventricular septum was assessed on the mid-chamber short axis images. Interventricular septal angle (ISA) was measured by determining the angle between the mid-point of the interventricular septum and the two hinge points. These CT measurements were performed on a commercially available workstation (Aquarius Net; TeraRecon, San Mateo, CA).

## Image analysis

CTPA scans were pre-processed with lung volume segmentation using multi-atlas based methods. Three atlases that were labeled semi-automatically by pulmonary experts using Pulmo-CMS software (17) were registered to each CTPA scan with Elastix (18). Majority voting was used to fuse the labels and extract the final lung segmentation. Pulmonary vessels were extracted within the lung volume, using a graph-cuts based method (19), where the vessel-likelihood (so-called “vesselness”, measured by the strain-energy filter (20)) and CT intensity were combined into a single cost function. Both pulmonary arteries and veins were included as the entire pulmonary vascular trees.

For each patient, pairwise image registration was employed between CT images of post- and pre-BPA, , using Elastix, as reported previously (21). The volume correction in this method was originally designed for parenchymal areas only, as a measure to correctly assess emphysema progression, where a proportional local increase in volume (estimated by the determinant of the Jacobian) was compensated by a proportional decrease in density (called the ‘dry sponge model’):

$$\Delta D(\boldsymbol{x}) = I_{post}\big(\boldsymbol{T}(\boldsymbol{x})\big) - I_{pre}(\boldsymbol{x}) \cdot [det\boldsymbol{J}_{\boldsymbol{T}}(\boldsymbol{x})]^{-1}\,, \qquad [1]$$

where $\Delta D(\boldsymbol{x})$ is the estimated density change at position $\boldsymbol{x}$; $I_{pre}(\boldsymbol{x})$ and $I_{post}(\boldsymbol{x})$ are the image intensities of the pre- and post-BPA CT scan; $\boldsymbol{T}(\boldsymbol{x})$ is the transformation function from the image registration, mapping the

coordinate $\boldsymbol{x}$ in the pre-BPA scan to the corresponding position in the post-BPA scan; and $det\boldsymbol{J_T}(\boldsymbol{x})$ is the determinant of the Jacobian of the transformation field at position $\boldsymbol{x}$.

As the 'dry sponge model' is not applicable for the pulmonary areas with high density, where pure liquid in pulmonary vessels is not compressible, we modified the model to restrict the scaling factor ($det\boldsymbol{J_T}(\boldsymbol{x})$) depending on the density. This so-called 'restricted sponge model' considers a voxel as composed of two components, air and liquid. Then density can be increased by leaving out the air component, and the density is only allowed to decrease by a maximum of 4 times the original volume of the air component (see Figure 1A). This means that the scaling factor is allowed to range from 0 to 4, if a voxel contains only air. For a voxel containing 100% water, blood or contrast agent (i.e. densities higher than 1000 gram/L) which is not compressible, then the scaling factor is set to 1. And for voxels with original densities between 0 and 1000 gram/L, linear lower and upper bounds for the scaling factor are used (see Figure 1B). Therefore, the sponge model in Equation [1] was modified as follows:

$$\Delta D(\boldsymbol{x}) = I_{post}\big(\boldsymbol{T}(\boldsymbol{x})\big) - I_{pre}(\boldsymbol{x}) \cdot max\left\{\theta_{min}\left(I_{pre}(\boldsymbol{x})\right), min\left\{\theta_{max}\left(I_{pre}(\boldsymbol{x})\right), det\boldsymbol{J_T}(\boldsymbol{x})\right\}\right\}^{-1}, \quad [2]$$

where $\theta_{min}$ and $\theta_{max}$ are the linear lower and upper bound, respectively.

In order to eliminate the dependence on a perfect matching quality between follow-up and baseline at the vascular boundary regions, we extracted only the centerlines of vessels by the symmetric distance transform method (DtSkeletonization method of Mevislab 2.7 (22)). Subsequently, only the voxels on the vascular centerlines were used for quantifying the density changes which were estimated with Equation 2. For visualization, the 'densitometric change' map was displayed as color-coded overlays as shown in Figure 2 (a, d) and 3D color-coded vascular centerlines were generated, as illustrated in Figure 2 (b, e). For quantification, the median and inter-quartile range (IQR) of the vascular densitometric changes (ΔVD) were calculated, as shown in Figure 2 (c, f), which were used to quantify the perfusion changes within vessels. The densitometric changes in parenchyma (ΔPD) were measured at the location of parenchymal 'centerlines' which are the parenchymal areas distal to pulmonary vessels. Similarly, the perfusion changes in pulmonary parenchyma were quantified by the median and IQR of the ΔPD.

## Statistical analysis

Continuous variables of the patient characteristics are presented as the median and interquartile range, and categorical variables are presented as frequencies and percentages. The normality of each variable was tested with a Shapiro-Wilk test and a normal Q-Q plot. The changes in RHC parameters, 6MWD, BNP levels, MTT, RV/LV ratio, PA diameter, ISA and density measurements between pre- and post-BPA were tested using the paired t-test or the Wilcoxon signed-rank test, as appropriate. Correlations between hemodynamic changes, 6MWD, BNP and densitometric changes were evaluated using Spearman's correlation coefficient. All statistical computations were performed in SPSS (Version 20.0. Armonk, NY: IBM Corp.). A 2-tailed p-value<0.05 was considered to be statistically significant.

# Results

The changes in RHC parameters, 6MWD, BNP, MTT, RV/LV ratio, PA diameter, ISA and perfusional quantifications between pre- and post-BPA are shown in Table 1. The hemodynamic parameters were improved by the BPA treatment, with a statistically significant decrease in sPAP, dPAP, mPAP and PVR. The 6MWD, BNP, RV/LV ratio and PA diameter were also significantly improved by the BPA treatment. The median densities decreased within the vascular trees after BPA, as quantified by automatic comparative imaging analysis (see Table 1). In the parenchyma on the other hand, the median densities did not change significantly.

The results of Spearman's correlation analysis between change in RHC parameters and change in densities are provided in Table 2. The IQR of ΔVD was significantly negatively correlated with all RHC parameters: ΔsPAP (R=-0.58, p=0.03), ΔdPAP (R=-0.71, p=0.005), ΔmPAP (R=-0.71, p=0.005) and ΔPVR (R=-0.77, p=0.001), which indicates that a wider inter-quartile range of ΔVD histogram corresponds to a larger decrease in both PAP and PVR after BPA treatment. Scatter plots of the hemodynamic changes and IQR of ΔVD are presented in Figure 3, among which the significant association between ΔPVR and IQR of ΔVD was particularly strong. Besides, the median of ΔPD was significantly correlated with both ΔdPAP (R=-0.58, p=0.030) and ΔmPAP (R=-0.59, p=0.025), which implies that the perfusion changes of pulmonary parenchyma could partly reflect the hemodynamic parameters changes. The Δ6MWD was significantly correlated with the Median of

ΔVD (R=-0.67, p=0.012), and ΔBNP had a significant correlation with the IQR of ΔPD (R=-0.645, p=0.013).

## Discussion

We studied the pulmonary perfusion changes in CTPA of CTEPH patients before and after BPA treatment. The CTPA before and after BPA treatment were compared by an automatic and objective method for identifying the perfusion changes in pulmonary vessels and parenchyma. The median and IQR of perfusion changes in pulmonary vessels and parenchyma were validated against RHC parameters changes. The IQR of ΔVD were significantly correlated with all PAP measurements and PVR, indicating that the hemodynamic changes could be reflected by perfusion changes. Furthermore, the color-coded visualization can offer insight into localized differences in BPA treatment effect.

The variety in perfusion changes in pulmonary vessels was quantitatively assessed by IQR of ΔVD, as it reflects the spread of both decrease and increase in density within pulmonary vessels. Vessels proximal to an obstruction ('upstream vessels') react differently to BPA treatment than vessels distal to obstruction ('downstream vessels'). Due to the obstructions in pulmonary arteries before treatment, contrast medium would accumulate in the 'upstream vessels' where hypertension leads to dilation and increased density in CTPA. The 'downstream vessels', however, are initially not reached by contrast medium and their densities in CTPA would therefore be lower than normal. When obstructions have been treated by BPA, the distribution of contrast medium through the pulmonary vascular system may be normalized. Therefore, the contrast medium is distributed more homogeneously after BPA, i.e. the densities in 'upstream vessel' would have decreased and densities in 'downstream vessels' would have increased after treatment. Thus, a wider range in ΔVD implies more equalization of contrast medium in vessels, i.e. more hemodynamic improvements.

In order to demonstrate the visualization of the changes in the quantified parameters, two patients with different outcomes after BPA were selected. According to RHC assessments, patient B had a larger decline in PAP and PVR after BPA treatment in comparison with patient A. As shown in the histogram of vascular densitometric changes, the IQR of patient B is wider than patient A. In the color-coded 2D visualization (Figure 2a and 2d), most of the vascular tree in patient A is coded in green, whereas in patient B more blue- and red-

coded vessels are displayed. This implies that perfusion changes in patient B are more widely spread, i.e. a better treatment effect.

In the pulmonary parenchyma, the hemodynamic changes obtained from RHC were reflected by the median ΔPD, not by the IQR of ΔPD. Due to the poor performance of the pulmonary vascular system before BPA treatment, transport of contrast medium to the parenchymal areas may be limited. After the BPA treatment, the performance of the vascular system might have been improved. Thus, instead of the variation in ΔPD, the median of ΔPD will provide insights into the perfusion changes in pulmonary parenchyma. The median of ΔPD was not significantly different from 0, while it was significantly correlated with ΔdPAP and ΔmPAP. The median of ΔPD did not change on average, however, its increases/decreases in an individual patient might moderately reflect the changes in RHC parameters. Although the information from ΔPD quantifications is not as clear as that from ΔVD, investigating changes in the pulmonary parenchyma shows potential.

Recently, several studies demonstrated the significant treatment effect of BPA by cautiously limiting the number of balloon inflations and target segments per session, and thus reducing the incidence of adverse complications, such as reperfusion edema and pulmonary bleeding (1). This procedure was added to treatment algorithms in the ESC/ERS guideline (23). However, its efficacy for long-term prognosis has not been established yet. In our clinical setting as an experienced CTEPH center, though rare, there are patients demonstrating re-exacerbation of CTEPH, year(s) after completion of BPA treatment courses. Considering the features of BPA procedure and patients' clinical course, several follow-ups are necessary in the management of patients with CTEPH. Our results provided objective and quantitative changes of pulmonary perfusion after BPA along with densitometry information on CTPA, which were correlated with invasive RHC exams.

Some previous studies have reported methods for estimating the severity of CTEPH. A study (24) validated automatic quantification of pulmonary perfused blood volume (PBV) with cardiac index, PAP, PVR, and 6MWD in 25 CTEPH patients. The PBV had negative significant correlations with sPAP and mPAP, but not significant with PVR, CI and 6MWD. In another study (15), authors manually measured lung PBV to correct the influence of artifacts and evaluated the PBV with PAP, PVR and RVP for 46 CTEPH patients. The lung PBV was significantly correlated with sPAP, dPAP, mPAP and PVR. The manually measured PBV might be used as a

non-invasive estimator of clinical CTEPH severity, however, reproducibility and objectivity of manual visual evaluations are generally poor. The pulmonary vascular morphology was investigated as an imaging biomarker for CTEPH in a recent study (25), in which the ratio of small-vessels volume (blood volume of vessels with a cross-sectional area of ≤ 5mm$^2$ , BV5) and total blood vessel volume (TBV) was measured for small-vessels pruning, and the ratio of large-vessels (a cross-sectional area of >10mm$^2$ , BV>10) and TBV was quantified for large-vessels dilation. The measurements were extracted in CTPA for 18 patients with CTEPH and 15 control patients. The quantifications of BV5/TBV and BV>10/TBV were significantly different between the CTEPH and control group, implying that pulmonary vascular morphology was remodeled by CTEPH. The pulmonary vascular morphology may be used as an imaging biomarker to assess disease severity. In another study (26), the lung PBV was quantified by dual-energy CT in 8 female patients with CTEPH pre- and post-BPA treatment and corrected with pulmonary artery enhancement (lung PBV/PAenh). The pre- to post-BPA improvements in both-lung PBV/PAenh had significant positive correlations with PAP, PVR and 6-minute walking distance, which implied that the lung PBV might be an indicator of BPA treatment effect. Optical Coherence Tomography (OCT) was used to classify the morphologies of 43 lesions in 17 patients pre- and post-BPA in another study (27). The newly proposed OCT-based morphologic lesion classification was evaluated to the pressure ratio and compared with conventional angiographic findings, which proved to be promising to predict accurate estimation of lesion responsiveness to BPA. In this study, the IQR of ΔVD can be used as a measurement to assess the treatment effect and additionally offers color-coded visualization back to CTPA. Furthermore, we compared CTPA before and after treatment, which offers insight into the treatment effect.

There are some limitations in our study. The quantifications were performed on both lungs together. More specific analysis of separate lungs or lung lobes may provide a more localized and accurate assessment of perfusion changes. We did not obtain an echocardiogram or MRI data along with the CT exam to evaluate cardiac output. The post contrast attenuation was not normalized for intra-individual variations that might be influenced by cardiac output. In the present study, the arteries and veins were not analyzed separately with an automatic method, whereas perfusion changes may differ between arteries and veins. A separated analysis of arteries and veins may therefore further improve the correlation. Nevertheless, even without these particular analyses, we already found a highly significant association between perfusion changes and hemodynamic

changes. In the future, quantifying the vessels with lesions treated by BPA would be an interesting research topic, as automatic and objective quantifications of the lesion morphology could provide specific benefits for planning or assessing BPA treatment. The studied group was relatively small and only included CTEPH patients without a control group. The normal vascular perfusion in healthy people might contribute to enhance the understanding of relations between pulmonary vascular perfusion and hemodynamic parameters. However, the method still offers insight into the variance in BPA treatment effects.

In conclusion, PAP and PVR were significantly improved after BPA, in the studied patient group with inoperable CTEPH. We assessed the perfusion changes in pulmonary vasculature achieved by BPA using an automatic comparison of CTPAs acquired before and after treatment. The IQR of ΔVD is associated with hemodynamic changes and can be used as a non-invasive measurement for assessing BPA treatment effects. The color-coded visualization provides insight into local differences in BPA treatment effects.

# Reference


1. Hoeper MM, Mayer E, Simonneau G, Rubin LJ**.** Chronic thromboembolic pulmonary hypertension. Circulation. 2006;113(16):2011-20.
2. Lang IM, Madani M**.** Update on chronic thromboembolic pulmonary hypertension. Circulation. 2014;130(6):508-18.
3. Lewczuk J, Piszko P, Jagas J, et al. Prognostic factors in medically treated patients with chronic pulmonary embolism. CHEST Journal. 2001;119(3):818-23.
4. Riedel M, Stanek V, Widimsky J, Prerovsky I**.** Longterm follow-up of patients with pulmonary thromboembolism: late prognosis and evolution of hemodynamic and respiratory data. Chest. 1982;81(2):151-8.
5. Mayer E, Jenkins D, Lindner J, et al. Surgical management and outcome of patients with chronic thromboembolic pulmonary hypertension: results from an international prospective registry. The Journal of thoracic and cardiovascular surgery. 2011;141(3):702-10.
6. Sugimura K, Fukumoto Y, Satoh K, et al. Percutaneous transluminal pulmonary angioplasty markedly improves pulmonary hemodynamics and long-term prognosis in patients with chronic thromboembolic pulmonary hypertension. Circulation Journal. 2012;76(2):485-8.
7. Madani MM, Auger WR, Pretorius V, et al. Pulmonary endarterectomy: recent changes in a single institution's experience of more than 2,700 patients. The Annals of Thoracic Surgery. 2012;94(1):97-103.
8. Mizoguchi H, Ogawa A, Munemasa M, et al. Refined balloon pulmonary angioplasty for inoperable patients with chronic thromboembolic pulmonary hypertension. Circulation: Cardiovascular Interventions. 2012;5(6):748-55.
9. Kim NH, Delcroix M, Jenkins DP, et al. Chronic Thromboembolic Pulmonary Hypertension. Journal of the American College of Cardiology. 2013;62(25 Supplement):D92-D9.
10. Reesink HJ, van der Plas MN, Verhey NE, et al. Six-minute walk distance as parameter of functional

outcome after pulmonary endarterectomy for chronic thromboembolic pulmonary hypertension. The Journal of thoracic and cardiovascular surgery. 2007;133(2):510-6.

11. Reesink HJ, Tulevski II, Marcus JT, et al. Brain natriuretic peptide as noninvasive marker of the severity of right ventricular dysfunction in chronic thromboembolic pulmonary hypertension. The Annals of thoracic surgery. 2007;84(2):537-43.

12. Liu M, Ma Z, Guo X, et al. Computed tomographic pulmonary angiography in the assessment of severity of chronic thromboembolic pulmonary hypertension and right ventricular dysfunction. European journal of radiology. 2011;80(3):e462-e9.

13. Ley S, Ley-Zaporozhan J, Pitton MB, et al. Diagnostic performance of state-of-the-art imaging techniques for morphological assessment of vascular abnormalities in patients with chronic thromboembolic pulmonary hypertension (CTEPH). European Radiology. 2012;22(3):607-16.

14. Krissak R, Henzler T, Reichert M, et al. Enhanced visualization of lung vessels for diagnosis of pulmonary embolism using dual energy CT angiography. Investigative radiology. 2010;45(6):341-6.

15. Takagi H, Ota H, Sugimura K, et al. Dual-energy CT to estimate clinical severity of chronic thromboembolic pulmonary hypertension: Comparison with invasive right heart catheterization. European Journal of Radiology. 2016;85(9):1574-80.

16. Fuster V**.** Hurst's the heart: McGraw-Hill Medical; 2008.

17. Stoel BC, Stolk J**.** Optimization and standardization of lung densitometry in the assessment of pulmonary emphysema. Investigative radiology. 2004;39(11):681-8.

18. Klein S, Staring M, Murphy K, et al. Elastix: a toolbox for intensity-based medical image registration. IEEE transactions on medical imaging. 2010;29(1):196-205.

19. Zhai Z, Staring M, Stoel BC**.** Lung vessel segmentation in CT images using graph cuts. SPIE Medical Imaging, 2016. International Society for Optics and Photonics: 97842K-K-8.

20. Xiao C, Staring M, Shamonin D, et al. A strain energy filter for 3D vessel enhancement with application to pulmonary CT images. Medical image analysis. 2011;15(1):112-24.

21. Staring M, Bakker M, Stolk J, et al. Towards local progression estimation of pulmonary emphysema using CT. Medical physics. 2014;41(2).

22. Selle D, Preim B, Schenk A, Peitgen H-O**.** Analysis of vasculature for liver surgical planning. IEEE transactions on medical imaging. 2002;21(11):1344-57.
23. Galiè N, Humbert M, Vachiery J-L, et al. 2015 ESC/ERS Guidelines for the diagnosis and treatment of pulmonary hypertension. European heart journal. 2015:ehv317.
24. Meinel F, Graef A, Thierfelder K, et al. Automated quantification of pulmonary perfused blood volume by dual-energy CTPA in chronic thromboembolic pulmonary hypertension. RöFo-Fortschritte auf dem Gebiet der Röntgenstrahlen und der bildgebenden Verfahren, 2014. © Georg Thieme Verlag KG: 151-6.
25. Rahaghi F, Ross J, Agarwal M, et al. Pulmonary vascular morphology as an imaging biomarker in chronic thromboembolic pulmonary hypertension. Pulmonary circulation. 2016;6(1):70.
26. Koike H, Sueyoshi E, Sakamoto I, et al. Quantification of lung perfusion blood volume (lung PBV) by dual-energy CT in patients with chronic thromboembolic pulmonary hypertension (CTEPH) before and after balloon pulmonary angioplasty (BPA): preliminary results. European journal of radiology. 2016;85(9):1607-12.
27. Inohara T, Kawakami T, Kataoka M, et al. Lesion morphological classification by OCT to predict therapeutic efficacy after balloon pulmonary angioplasty in CTEPH. International journal of cardiology. 2015;197:23-5.

# Tables

**TABLE 1.** Changes in hemodynamic parameters, 6MWD, BNP, MTT, RV/LV ratio, PA diameter, ISA and densitometry

| | Pre-BPA | Post-BPA | Change | p-value |
|---|---|---|---|---|
| RHC parameters | | | | |
| sPAP (mmHg) | 60.5 ± 33 | 36 ± 19 | 23 ± 19 | 0.002 |
| dPAP (mmHg) | 20 ± 16 | 12.5 ± 11 | -5 ± 11 | 0.006 |
| mPAP (mmHg) | 34.5 ± 17 | 21.5 ± 15 | -12.5 ± 14 | 0.003 |
| PVR (dyne·s/cm$^5$) | 496 ± 396 | 246 ± 185 | -185 ± 409 | 0.004 |
| 6MWD (m) | 450 ± 159 | 510 ± 95 | 50 ± 115 | 0.004 |
| BNP (pg/ml) | 80.4 ± 160 | 26.8 ± 32.7 | -53.2 ± 146 | 0.01 |
| MTT (seconds) | 10.1 ± 2.95 | 9.95 ± 2.1 | -0.05 ± 2.08 | 0.31 |
| RV/LV ratio | 1.21 ± 0.53 | 1.05 ± 0.1 | -0.09 ± 0.28 | 0.005 |
| PA diameter (mm) | 30.1 ± 6.22 | 28.6 ± 5.54 | -1.9 ± 3.43 | 0.024 |
| ISA (degree) | 131 ± 11.8 | 130 ± 16.2 | -2.5 ± 27.5 | 0.397 |
| Density measurements (HU) | | | | |
| Median VD | -415 ± 101 | -433 ± 114 | -51.5 ± 20.8 | <0.001 |
| IQR of VD | 437± 73 | 475 ± 67 | 182 ± 60 | <0.001 |
| Median PD | -864 ± 47 | -861 ± 54 | -3.5 ± 22.5 | 0.379 |
| IQR of PD | 437 ± 73 | 475 ± 67 | 45 ± 15 | <0.001 |

sPAP, systolic pulmonary artery pressure; dPAP, diastolic pulmonary pressure; mPAP, mean pulmonary artery pressure; PVR, pulmonary vascular resistance; 6MWD, 6-min walk distance; BNP, brain natriuretic peptide; MTT, mean transit time; RV/LV ratio, right ventricular short axis to left ventricular short axis ratio; PA diameter, diameter of pulmonary artery trunk; ISA, interventricular septal angle; IQR, inter-quartile range; VD, vascular density; PD, parenchymal density. See the online supplement for individual measurement results.

347

348

**TABLE 2.** Correlation R (p-value) analysis between RHC parameters, 6MWD, BNP and image-derived perfusion changes

| | Median of ΔVD | IQR of ΔVD | Median of ΔPD | IQR of ΔPD |
|---|---|---|---|---|
| ΔsPAP | 0.53 (0.054) | -0.58 (0.031) | -0.32 (0.263) | -0.18 (0.529) |
| ΔdPAP | 0.18 (0.536) | -0.71 (0.005) | -0.58 (0.030) | -0.40 (0.152) |
| ΔmPAP | 0.46 (0.095) | -0.71 (0.005) | -0.59 (0.025) | -0.37 (0.190) |
| ΔPVR | 0.28 (0.325) | -0.77 (0.001)* | -0.43 (0.121) | -0.36 (0.201) |
| Δ6MWD | -0.67 (0.012) | -0.011 (0.817) | -0.011 (0.971) | 0.48 (0.093) |
| ΔBNP | 0.10 (0.725) | -0.53 (0.052) | -0.39 (0.163) | -0.65 (0.013) |

* significance level obtained after Bonferroni correction for multiple testing.

349

# Figure legends

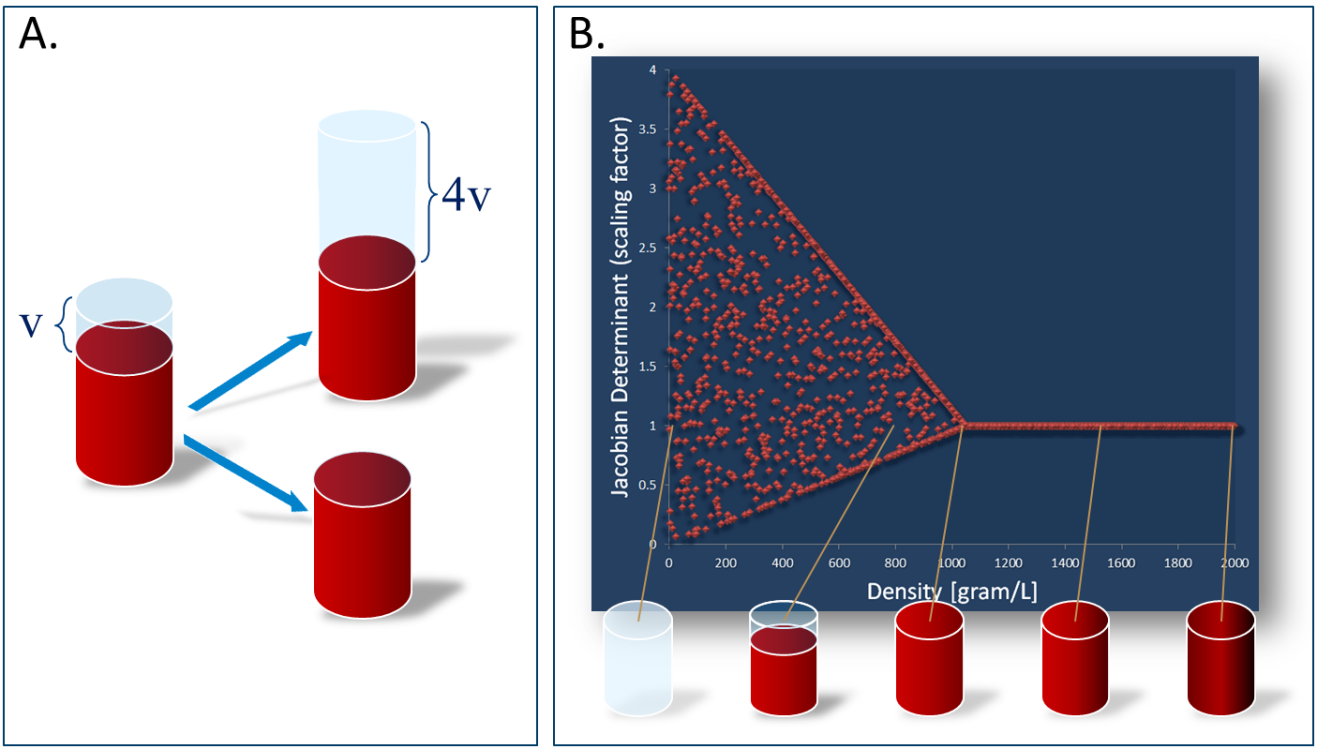


FIGURE 1. A) Two-component model: a voxel is composed of an air and blood compartment (or water or contrast agent), where density increase is restricted to the situation where all air has been expired, or where there is a 4 fold increase of the amount of inspired air. B) The scaling factor from the determinant of the Jacobian is thus restricted by an upper and lower limit depending on the density of a voxel.

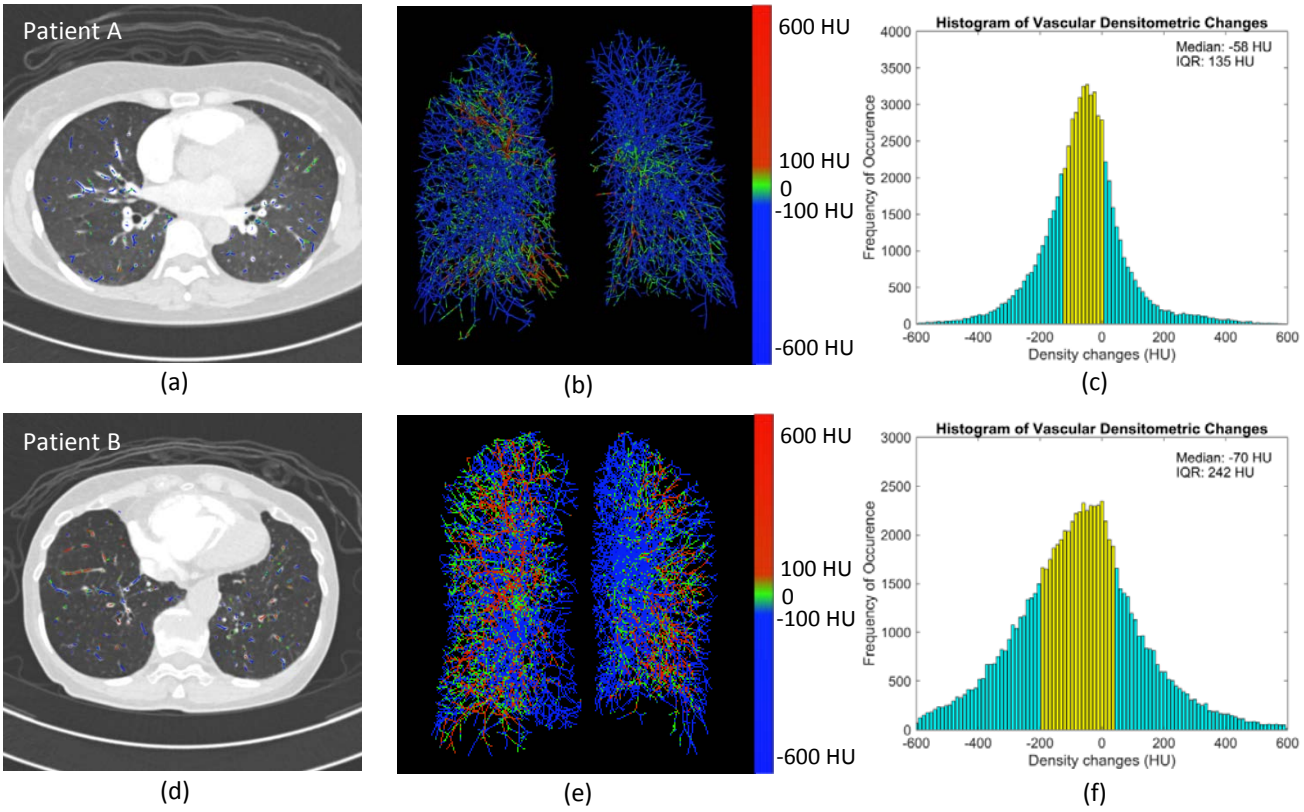


356

357 FIGURE 2. Vascular densitometric changes of two patients. (a, d) one slice of CTPA with color-coded overlay of
358 vascular densitometric changes; (b, e) 3D color-coded visualization of vascular centerlines; (c, f) histogram of
359 vascular densitometric changes and yellow bins representing vascular densitometric changes within the IQR.
360 Patient A and B had a decrease in mPAP by -3 and -34 mmHg, respectively and a decrease in PVR by -39
361 and -734 dyne·s/cm$^5$, respectively.

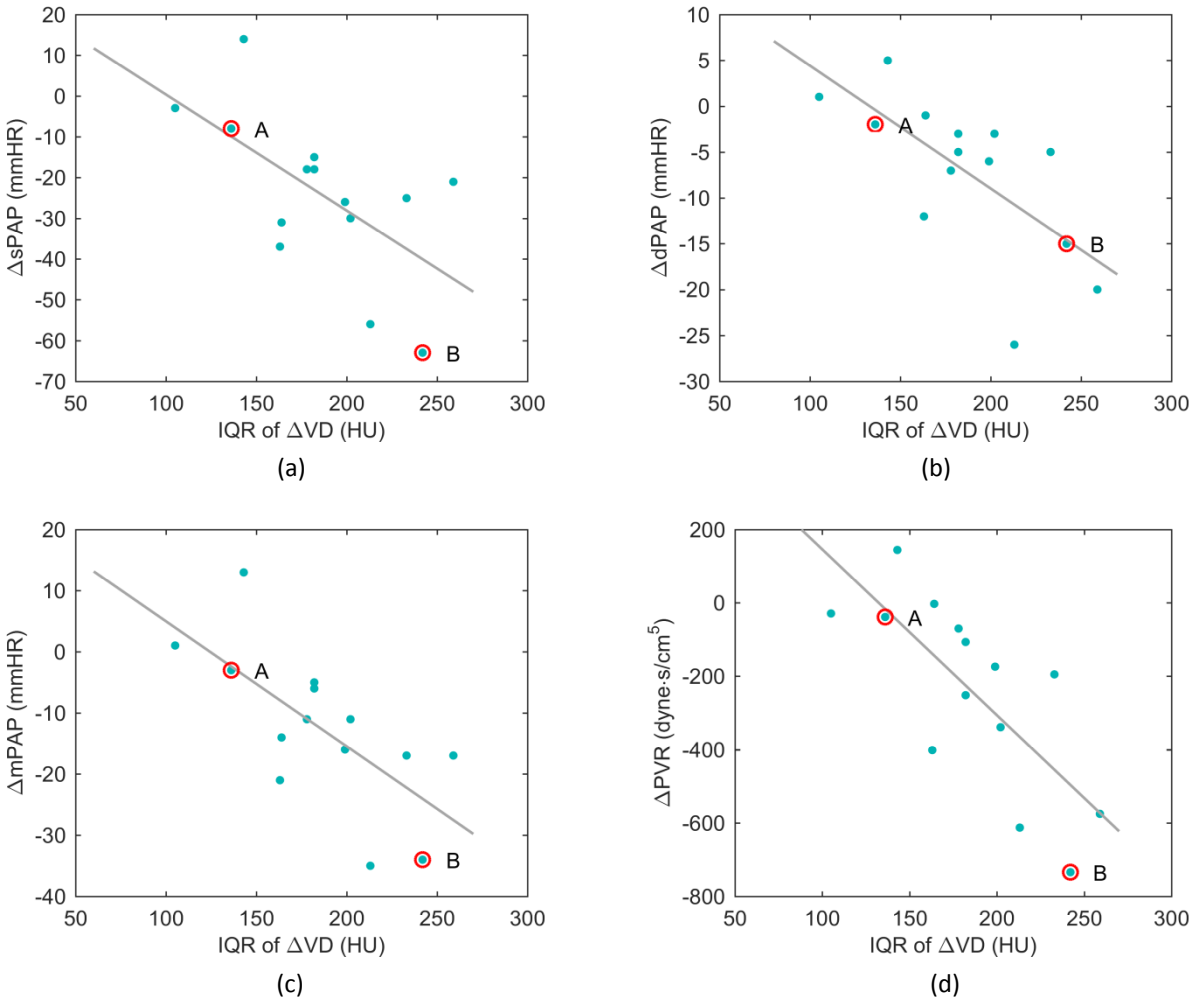


362

363 FIGURE 3. Correlation between IQR of ΔVD and RHC parameters (A and B are corresponding to patient A and
364 B in Figure 2, respectively). (a) Correlation between IQR of ΔVD and ΔsPAP (R=-0.58, p-value=0.031); (b)
365 Correlation between IQR of ΔVD and ΔdPAP (R=-0.71, p-value=0.005); (c) Correlation between IQR of ΔVD
366 and ΔmPAP (R=-0.71, p-value=0.005); (d) Correlation between IQR of ΔVD and ΔPVR (R=-0.77, p-
367 value=0.001).

368